

## Article

# Influence of the Iron as a Dopant on the Refractive Index of WO<sub>3</sub>

Mariana Osiac<sup>1</sup>, Iulian Boerasu<sup>2</sup> , Madalin-Stefan Radu<sup>1</sup> , Maria Jigau<sup>1</sup> and Ion Tirca<sup>1,\*</sup>

- <sup>1</sup> Department of Physics, Faculty of Sciences, University of Craiova, 200585 Craiova, Romania; mariana71osiac@gmail.com (M.O.); madalin.radu17@gmail.com (M.-S.R.); mariajigau@mail.ru (M.J.)
- <sup>2</sup> Department of Lasers, Plasma and Radiation Physics, National Institute for Lasers, 077125 Magurele, Romania; iulian.boerasu@inflpr.ro
- \* Correspondence: tirca.ionut2009@gmail.com

**Abstract:** Results on studies of pure tungsten oxide WO<sub>3</sub> and 2, 3 and 4% Fe-doped WO<sub>3</sub> grown on the sapphire substrates by reactive pulsed laser deposition technique are reported. From X-ray diffraction it results that the crystalline structures changed with the substrate temperature and the peaks diffraction having a small shift by the amount of Fe content in WO<sub>3</sub> lattice was noticed. Scanning electron microscopy presented a random behavior of WO<sub>3</sub> nanocrystallites size with substrate temperatures. In the presence of 2% Fe-doped WO<sub>3</sub>, the nanocrystallites size varied gradually from 60 nm to 190 nm as substrate temperature increased. The transmission spectra of the pure and 2, 3 and 4% Fe-doped WO<sub>3</sub> films were obtained within the 300–1200 nm spectral range. The refractive index of WO<sub>3</sub> and Fe-doped WO<sub>3</sub> layers were calculated by the Swanepoel method. The refractive index of pure WO<sub>3</sub> shows a variation from 2.35–1.90 and for 2% Fe-doped WO<sub>3</sub> from 2.30–2.00, as the substrate temperature increased. The contents of 3 and 4% Fe-doped WO<sub>3</sub> presented nearly identical values of the refractive index with pure and 2% Fe-doped WO<sub>3</sub>, in error limits, at 600 °C. The optical band gap changes with substrate temperature from 3.2 eV to 2.9 eV for pure WO<sub>3</sub> and has a small variation with the Fe.

**Keywords:** thin film; pure and 2% Fe-doped tungsten oxide; refractive index; optical band gap



**Citation:** Osiac, M.; Boerasu, I.; Radu, M.-S.; Jigau, M.; Tirca, I. Influence of the Iron as a Dopant on the Refractive Index of WO<sub>3</sub>. *Materials* **2021**, *14*, 5845. <https://doi.org/10.3390/ma14195845>

Academic Editor: Sergej Kulnich

Received: 4 August 2021  
Accepted: 30 September 2021  
Published: 6 October 2021

**Publisher's Note:** MDPI stays neutral with regard to jurisdictional claims in published maps and institutional affiliations.



**Copyright:** © 2021 by the authors. Licensee MDPI, Basel, Switzerland. This article is an open access article distributed under the terms and conditions of the Creative Commons Attribution (CC BY) license (<https://creativecommons.org/licenses/by/4.0/>).

## 1. Introduction

Tungsten trioxide (WO<sub>3</sub>) is an important n-type semiconductor with excellent properties for electrochromic devices, gas sensing, heterogeneous catalysts, chromogenic devices, solar energy devices, field electron emission, etc.

The sensors based on WO<sub>3</sub> are highly sensitive for very low concentrations of toxic gases such as NO<sub>x</sub>, H<sub>2</sub>S, NH<sub>3</sub> and CO [1–5]. Moreover, WO<sub>3</sub> films with transparent characteristics in the visible region are of interest in electrochromic phenomena for applications in display devices or smart windows [6]. The sub-stoichiometric intermediate phases make WO<sub>3</sub> appropriate for electronic properties such as superconductivity and ability to carry a charge. The WO<sub>3</sub> metal oxide nanowires have a great importance because of their distinctive electrochromic, optochromic, gas chromic and magnetic properties. Thus WO<sub>3</sub> metal oxide nanowires have become good candidates for lithium-ion batteries, catalysts, electrochromic devices and sensors. The metal oxide nanowires provide a unique system for understanding superconductivity and colossal magnetoresistance properties [7–10], therefore WO<sub>3</sub> nanowires have been produced by different methods [11]. Regarding the sensor applications, some limitations appear, such as high operating temperature, slow response time, and poor selectivity and reproducibility, making them impractical monitors for area air quality and safety. To overcome these limitations, research attention has been focused on increasing the sensor performance, which is usually realized by the incorporation of metals in the base metal oxide sensors.

With respect to other deposition techniques, pulsed laser deposition (PLD) allows control of the layer properties by adjusting various parameters such as laser fluence, substrate temperature, or gas pressure. The growth of WO<sub>3</sub> thin films by PLD in an oxygen atmosphere was firstly reported by Poniatowski et al. [12]. Deposition of pure and doped WO<sub>3</sub> layers with noble metals has been mainly done by the PLD method [13–17].

The WO<sub>3</sub> thin films and nanostructures used for technological applications need a study of the optical properties such as refractive index and optical band gap. The optical characterization of thin films can be determined by the Swanepoel method [18]. This method uses the envelopes on the interference fringes obtained by the transmission spectra of films grown on thick transparent substrates [19–21]. The two-term Cauchy dispersion function was used to fit the refractive index obtained from the transmission spectra. The transmission spectra was done in the 300–1200 nm wavelength range. By means of the Swanepoel method the refractive index has been calculated taking into account the values of  $T_{max}(\lambda)$  and  $T_{min}(\lambda)$  of the transmission spectra.

The choice of the range 300–1200 nm is done by the fact that above the 1200 nm the maximum and minimum peaks become very rare and wide and leads to refractive index values far outside the error limit and implicitly to a totally wrong approximation.

In order to improve the optical properties of WO<sub>3</sub> layer, several concentrations of the dopant (2, 3 and 4% Fe) were chosen and investigated at various temperatures. It was found that the concentration of 2% Fe was close to pure WO<sub>3</sub> crystalline structure.

The goal of this paper is to measure refractive indexes in the 300–1200 nm spectral range of pure and 2, 3, 4% (weight) Fe-doped WO<sub>3</sub> thin films deposited by PLD on the sapphire substrate by using the Swanepoel method. The refractive index was obtained for layers grown at various temperatures in the range 600–700 °C at 4 h deposition time. A comparison among the refractive indexes of pure and 2% Fe-doped WO<sub>3</sub> layers was done. The optical properties such as optical band gap have been measured. The relationship between the crystalline structure and the morphology of the film surface has been investigated. The optical parameters, such as refractive index ( $n$ ), film thickness ( $d$ ), or optical band gap ( $E_g$ ) for the films prepared at different temperatures are obtained from the corresponding transmission spectra.

## 2. Material and Methods

### *Thin Film Investigation Methods*

The pure and 2, 3 and 4% Fe-doped WO<sub>3</sub> thin films were grown on sapphire substrates by PLD [10–15]. An Nd-YAG laser (266 nm laser wavelength) with a repetition rate of 10 Hz and a pulse duration of 10 ns was used. The diameter of the laser beam is approximately 1 mm and the energy was adjusted to obtain a fluence of approximately 1.7 J/cm<sup>2</sup>. The sapphire substrates were located at 4.5 cm from the targets (WO<sub>3</sub> and 2, 3, 4% Fe + WO<sub>3</sub>) and were radiative heated between 600–700 °C, with a heating rate of 15 °C/min. The deposition has been carried out in oxygen atmosphere, at a pressure of 120 mTorr.

A model 6000 X-ray diffraction system (Shimadzu, Tokyo, Japan) was used to investigate the crystalline structure of the pure and 2, 3 and 4% Fe-doped WO<sub>3</sub> samples.

A field emission scanning electron microscope (FE-SEM; Thermo Fisher Scientific, Waltham, MA, USA) coupled with a EDX (model ApreoSLoVachas, Hillboro, OR, USA) was used to study the surface morphology of samples. The plane view (0° tilt) samples surface and cross-section (90° tilt) morphology have been investigated in high-vacuum operation mode ( $6.1 \times 10^{-4}$  Pa) at a working distance of 10.5 mm, using 10 kV as accelerating voltage and a nominal electron beam current of 13 Pa. The SEM images were recorded on as-processed samples, i.e., without any conductive coatings.

The optical properties of pure and 2, 3, 4% Fe doped WO<sub>3</sub> films have been investigated by the Swanepoel method. The transmission spectra within the 200–1200 nm spectral range were recorded using a Specord 210 plus instrument (Analytik Jena AG, Jena, Germany) in scanning mode. The spectrophotometer was coupled with an integration sphere that ensures uniform illumination at a normal incidence of the light on the film surface (1 mm),

independent of the scattering or the deflection beam. The optical transmission measurements were done in the center of the samples. The oscillations within the transmission spectra indicate a source of optical interference. These oscillations are an effect of the pure and doped  $\text{WO}_3$  thin film and substrate. Applying the Swanepoel method the refractive index value of crystalline films was obtained. The Swanepoel method described briefly here takes into account the mathematical functions that envelope the transmittance spectra, which include multiple maxima and minima due to interference fringes. The sapphire substrates show a refractive index  $s$ , given by Equation (1):

$$s = \frac{1}{T_s} + \left( \frac{1}{T_s} - 1 \right)^{1/2} \quad (1)$$

where  $T_s$  is the transmittance of the sapphire relative to air.

The refractive index of pure and 2, 3 and 4% Fe-doped  $\text{WO}_3$  in the weak and medium absorption has been calculated taking into account the values of  $T_{max}(\lambda)$  and  $T_{min}(\lambda)$  from the transmittance spectra. The values of the refractive index of the pure and doped  $\text{WO}_3$  layers, in the first approximation, denoted by  $n_1$ , is calculated by the following expression:

$$n_1 = \left( N_1 + (N_1^2 - s^2)^{1/2} \right)^{1/2} \quad (2)$$

where  $N_1$  is a parameter depending on the  $T_{max}$  and  $T_{min}$  and substrate thickness,  $s$ , from Equation (1). Then film refractive index value  $n_1$  obtained by Equation (2) is improved after calculating the film thickness,  $d_1$ . By means of the basic equation of interference fringes, the film thickness is calculated as:

$$d_1 = \frac{\lambda_1 \lambda_2}{2(\lambda_1 n_{e2} - \lambda_2 n_{e1})} \quad (3)$$

with  $n_{e1}$  and  $n_{e2}$  the refractive indices at two successive maxima or minima corresponding to the wavelengths,  $\lambda_1$  and  $\lambda_2$ , respectively. The interference fringes equation is  $2nd = m_0\lambda$ , where  $m_0$  is the first approximation of  $m$ , which is an integer for maxima and a half-integer for minima. The exact value of  $m$  increases the film thickness accuracy. The new values of the thickness  $d_2$  are derived from Equation (3).

The final value of  $d_2$  is found after calculation of  $n_1$  by Equation (2). The film thickness accuracy is in the range of 1.1–3%. The refractive index values of pure and Fe doped  $\text{WO}_3$  films are calculated using the exact value  $m$  and the thickness,  $d_2$ . Finally, the refractive index values are fitted by a two-term Cauchy dispersion relation in the range of measurements:

$$n(\lambda) = B + \frac{C}{\lambda^2} \quad (4)$$

where,  $B$  and  $C$  are constants. In the calculation of  $d_2$  higher values of the layer thickness are not considered.

The optical band gap  $E_g$  has been determined from absorption coefficient data as a function of photon energy using the Tauc relation:

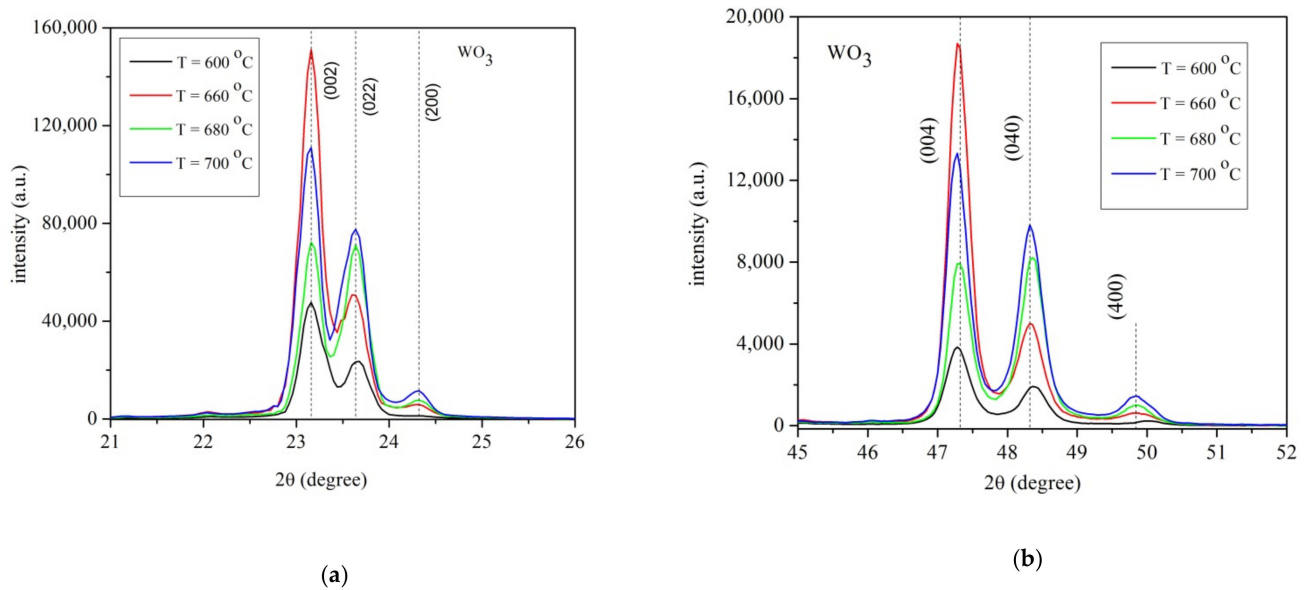
$$(\alpha h\nu)^{1/2} = A (h\nu - E_g) \quad (5)$$

where  $A$  is the slope of the Tauc edge, named band parameter, which might depends on the width of localized states in the bandgap. The ordinate is given by  $(\alpha h\nu)^{1/r}$ , where  $\alpha$  is the absorption coefficient, the exponent  $1/r$  denotes the nature of the transition and  $r$  may take the values  $\frac{1}{2}$ ,  $3/2$ ,  $2$ , or  $3$ , depending on the transitions being either direct allowed, direct forbidden, indirect allowed, or indirect forbidden, respectively. In the present case, the exponent is corresponds to the value  $r = 2$ , being an indirect allowed transition.

### 3. Results and Discussions

#### 3.1. X-ray Measurements

Figure 1a,b show the X-ray spectra for all samples in the  $2\theta = 21\text{--}52^\circ$  range. The samples present the  $\gamma$ -monoclinic crystalline structure (ICDD card No.043-1035) of the  $\text{WO}_3$  layer. The X-ray spectra of the layers deposited at temperatures 600, 660, 680 and 700 °C respectively (Figure 1a) presented diffraction peaks at (002), (022) and (200), with a preferential crystalline plane (002) along the c-axis. The intensities of the diffraction peaks (002), (022) for the sample grown at 680 °C are nearly identical.



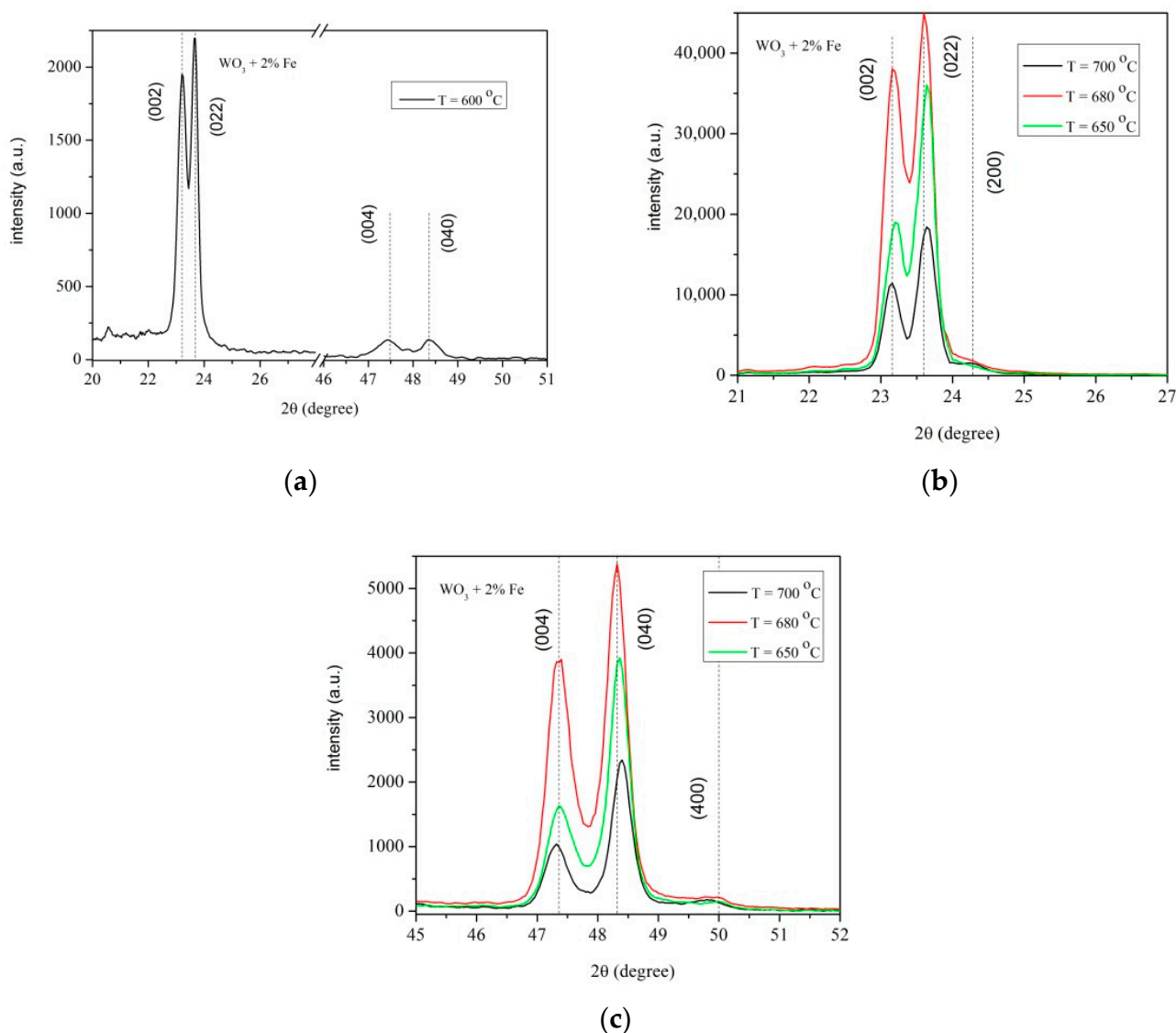
**Figure 1.** X-ray patterns for  $\text{WO}_3$  layers grown on sapphire substrate at temperatures  $T = 600^\circ\text{C}$ ,  $T = 660^\circ\text{C}$ ,  $T = 680^\circ\text{C}$ ,  $T = 700^\circ\text{C}$  and deposition time 4 h. (a) range  $2\theta = 21\text{--}26^\circ$ ; (b) range  $2\theta = 45\text{--}52^\circ$ .

Figure 1b illustrates the X-rays diffraction peaks for  $\text{WO}_3$  layers in the  $2\theta = 45\text{--}52^\circ$  range. The X-rays diffractions peaks are (004), (040), and (400), respectively. The layer grown at 660 °C has the highest intensities of the (004) diffraction peak. The intensities of the diffraction peaks are gradually increasing with temperatures an exception being at 660 °C. In the 640–660 °C range, the crystalline structure of the  $\text{WO}_3$  has the diffraction peaks intensities nearly identical, thus a random orientation of the monoclinic structure is presented.

Figure 2a–c present the X-ray spectra for all samples in the  $2\theta = 20\text{--}52^\circ$  range. The figures evidence the crystalline structure of 2% Fe-doped  $\text{WO}_3$  layer. The X-ray spectra of the layers grown at temperatures 600–700 °C (Figure 2a,b) exhibit characteristic diffraction peaks at (002), (022) with a preferential crystalline plane (022), i.e., b-axis.

In the XRD pattern of Figure 2a,b the intensity of peaks corresponding to (022) increases gradually at 600, 650 and 680 °C, respectively and strongly decreases at 700 °C. A gradual decreasing of the diffraction peaks intensities with increasing temperature is shown in Figure 2c.

In Figure 2a, the diffraction peak (200) of the layer grown at 600 °C vanishes, this effect being related to the small amount of Fe doped in the host lattice of  $\text{WO}_3$ .



**Figure 2.** (a–c) X-ray patterns of 2%Fe doped  $\text{WO}_3$  layers grown on sapphire substrate at various temperatures and 4 h deposition time (a)  $T = 600^\circ\text{C}$  in the range  $2\theta = 20\text{--}51^\circ$ ; (b)  $T = 650^\circ\text{C}$ ,  $T = 680^\circ\text{C}$ ,  $T = 700^\circ\text{C}$  in the range  $2\theta = 21\text{--}27^\circ$ ; (c)  $T = 650^\circ\text{C}$ ,  $T = 680^\circ\text{C}$ ,  $T = 700^\circ\text{C}$  in the range  $2\theta = 45\text{--}52^\circ$ .

The effect of Fe as a dopant is visible for 3% and 4%Fe doped  $\text{WO}_3$  layers. The diffraction peaks (022), (200), (040) and (400), respectively for 3 and 4% Fe doped  $\text{WO}_3$  layers vanished. To analyze the effect of Fe doped  $\text{WO}_3$  layer, the plots are made as a function of temperature for pure/doped  $\text{WO}_3$  for a better characterization, as seen in Figure 3a,b.

Figure 3a presents a small deviation of (200)/(022) diffraction peaks compared to pure  $\text{WO}_3$  with increasing the content of (2, 3, 4%) Fe-doped  $\text{WO}_3$ . A small deviation of diffraction peaks (004)/(040) of Fe-doped  $\text{WO}_3$  compare to pure  $\text{WO}_3$  is noticed in Figure 3b. This deviation is attributed to the ionic radius of octahedral coordinated  $\text{Fe}^{3+}$  of  $0.64 \text{ \AA}$ , close to that of  $\text{W}^{6+}$  with identical coordination number ( $0.60 \text{ \AA}$ ) [22,23]. The crystalline field stabilization energy of octahedral coordination for  $\text{Fe}^{3+}$  ion is higher than that of tetrahedral coordination. Thus,  $\text{Fe}^{3+}$  ions could enter in the host lattice of  $\text{WO}_3$  and replace  $\text{W}^{6+}$  ions. The difference of the ionic radius of octahedral coordinated ( $0.04 \text{ \AA}$ ) results in a small shift in peak positions observed in Figure 3a,b. The observed shift in peak positions of Fe-doped  $\text{WO}_3$  compared to pure  $\text{WO}_3$  can be attributed to the small difference between of  $\text{W}^{6+}$  and  $\text{Fe}^{3+}$  ionic radii. The  $\text{Fe}^{3+}$  ionic radius being a little greater

than that of  $W^{6+}$ , a slight distortion appeared in the crystal lattice when  $WO_3$  is doped with Fe, resulting in a shift in the diffraction peaks. The lattice distortions produce numerous defects in the film.

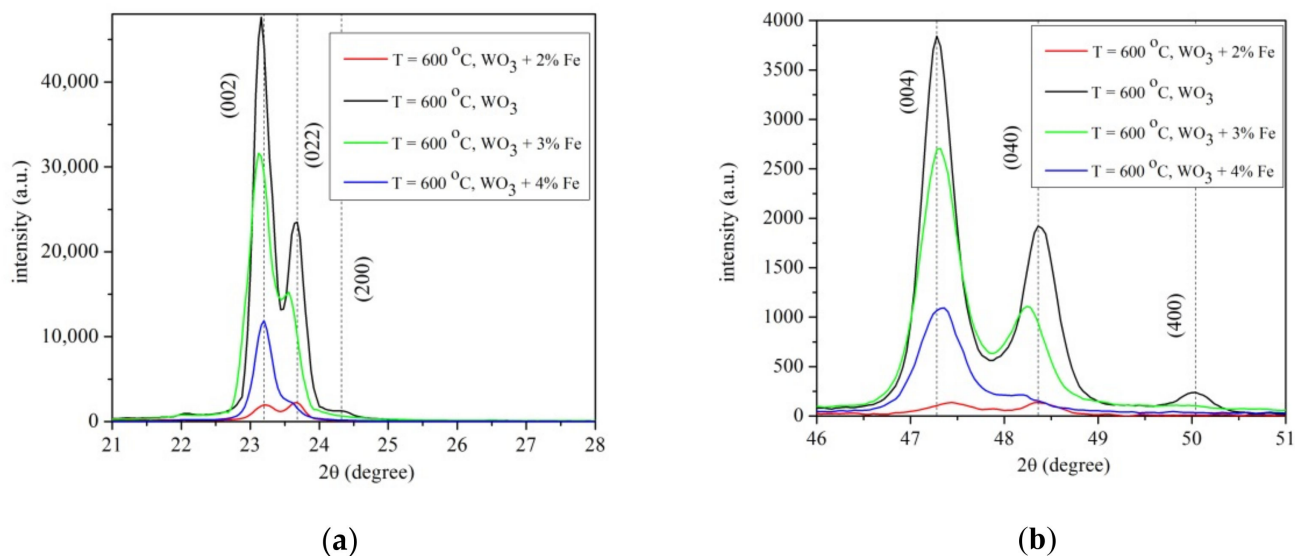


**Figure 3.** (a,b) X-ray pattern of pure and 2, 3 and 4% Fe doped  $WO_3$  layers grown on sapphire substrate at 4 h deposition time and substrate temperature  $T = 600$  °C. (a) pure and 2, 3 and 4% Fe doped  $WO_3$  in the range  $2\theta = 21$ – $28^\circ$ ; (b) pure and 2, 3 and 4% Fe doped  $WO_3$  in the range  $2\theta = 46$ – $51^\circ$ .

### 3.2. SEM Measurements

The top-view high magnification secondary electron (SE) images of pure  $WO_3$  and 2% Fe doped  $WO_3$  thin films as function of deposition temperature are shown in Figures 4 and 5.

According with the recorded images, the impact of the substrate temperature on the surface morphology of processed samples is important. Moreover, analyzing the recorded images, the surface morphology evolution seems having a random dependence on the substrate temperature increasing. Indeed, a rough nanostructured surface consisting in well-defined surface grain features illustrated the morphology of pure  $WO_3$  grown at 600 °C (Figure 1a). The observed  $WO_3$  grains are like pyramid-shaped, sharp grains with a size of approximately 130 nm and micro-holes are visible around the grains. A fine microstructure and uniform distribution of the particles are evident in the micrographs recorded on the pure  $WO_3$  films grown at 660 °C (Figure 1b). The grains are more homogeneous and compactly arranged than the grains observed in  $WO_3$  films grown at 600 °C. The average size of surface grains of those films is decreased to approximately 73 nm. Even low as volume fraction, micro-holes are observed preferentially located on the grain-boundaries. Further increasing the deposition temperature at 680 °C, the surface morphology of the growth films consists in grains of pyramidal shape, with a size of about 127 nm, randomly oriented with respect to the substrate surface. A large amount of physical defects, like micro-holes, are visible around the grains. Particularly, a surface morphology featured by grain size decreasing (average grain size of 97 nm), and rough rectangular-shaped grains were observed in the film grown at a substrate temperature of 700 °C. However, for those  $WO_3$  films, several nano-sized holes are distributed both on the grains, and at the grain boundaries.

The high magnification SEM images of 2% Fe-doped  $WO_3$  films depending on various temperatures are shown in Figure 5a–d.

The effect of temperature on the surface morphology of Fe-doped  $WO_3$  films is remarkable. The SEM data of 2% Fe-doped  $WO_3$  films can be divided into three temperature areas where the morphology differences are significant. The first area contains the 2% Fe-doped  $WO_3$  films grown at temperatures of 600 °C and 650 °C, respectively. In this

temperature area, the morphology of the deposited films has a “cobbled” appearance, with well-defined grains of an average size of about 60 nm. The second area of 2% Fe-doped  $\text{WO}_3$  films grown at temperatures of 650 °C and 680 °C, with a rough surface morphology, composed of slightly larger pyramid-shaped crystallites (average size of 90 nm) is observed. However, a large amount of physical defects like microporosity is obviously visible in the grains boundaries area. The third temperature area belongs to films grown at 700 °C. According to the recorded images, at 700 °C deposition temperature leads to a simultaneous increase of the size of the grain surface, and grain size homogeneity. The films grown at this temperature show a compact surface morphology formed by large pyramidal-shaped grains, with an average size of 194 nm. Nano-porosity located on the grains surface is visible in the recorded images.

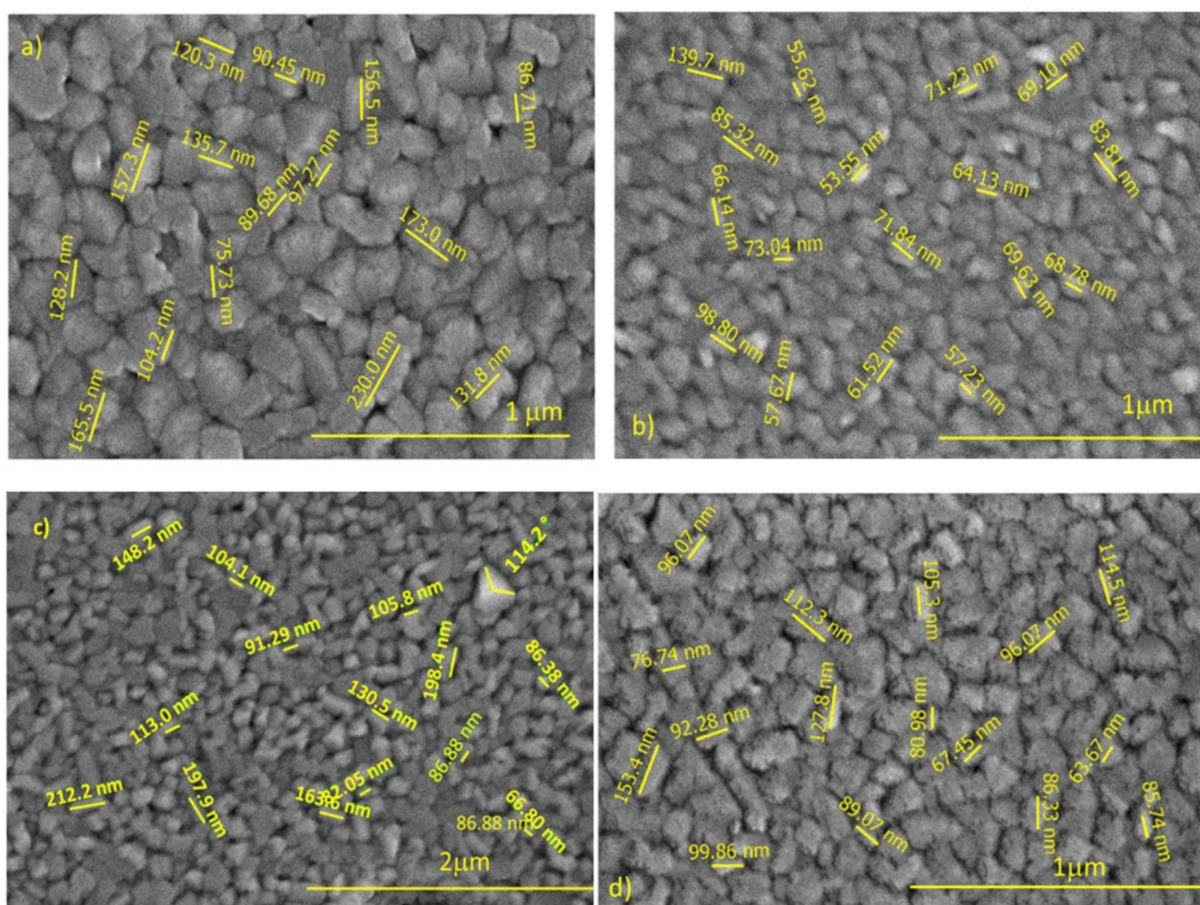


**Figure 4.** SEM image of the  $\text{WO}_3$  layer grown at 4 h deposition time and various temperatures. (a)  $T = 600$  °C; (b)  $T = 660$  °C; (c)  $T = 680$  °C and (d)  $T = 700$  °C.

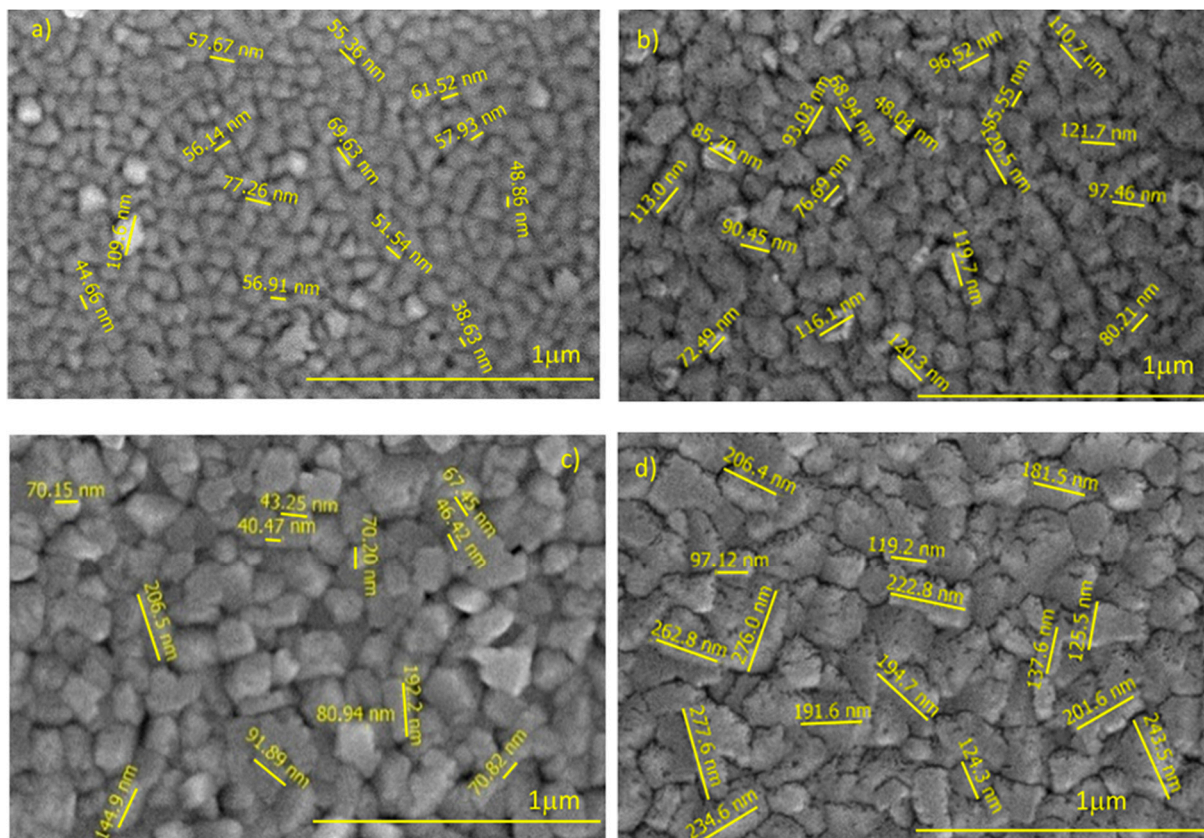


**Figure 5.** SEM image of the 2%Fe doped WO<sub>3</sub> layer grown at 4 h deposition time and various temperatures. (a) T = 600 °C; (b) T = 650 °C; (c) T = 680 °C and (d) T = 700 °C.

### 3.3. Refractive Index

The calculation of the refractive index from Equations (2) and (3) using the Swanepoel method are displayed in Tables 1 and 2 for two extreme temperatures (600 and 700 °C, respectively), particularly for the WO<sub>3</sub> + 2% Fe layer. The layer thicknesses with larger values are removed from the final calculation of  $d_2$  as is shown in Tables 1 and 2. The layer thickness calculated by the Swanepoel method and the thickness measured by SEM cross-section, in Tables 1 and 2 show good agreement. The refractive indexes and layer thickness for sample grown at 3 and 4% Fe-doped WO<sub>3</sub> are calculated in the similar way as for the samples with 2% Fe + WO<sub>3</sub>.

The graphs corresponding to the refractive index values  $n_2$  are presented in Figure 6a,b for the samples grown at 4 h substrate temperature in the range of 600 and 700 °C, respectively. The refractive index values obtained from the transmission spectra are fitted using a two-term Cauchy dispersion function in the wavelength range of 400–1200 nm.

In Tables 1 and 2, the final results of thickness,  $d_2$ , the refractive index, and the Cauchy dispersion are presented. The thickness values of  $d_2$  are derived from Equation (3) together with  $n_1$  calculated by Equation (2), and finally the values of  $d_2$  are obtained with good accuracy.

The values of the refractive index from Figure 6a,b are varied from 2.32–2.00 at 600 °C and 2.20–1.90 at 700 °C, respectively. The similar values of refractive index in this temperature range have been reported previously [24,25]. Considering the present work and the ref. [24], the refractive index values seem to be independent of the transparent substrates such as quartz and sapphire.

The refractive index of 2% Fe-doped WO<sub>3</sub> layer grown at 4 h deposition time at 600 °C presents values in the range 2.40–2.04, as shown in Figure 7a. The tiny amount of 2% Fe presents in the WO<sub>3</sub> layer does not significantly the refractive index change compared with



pure WO<sub>3</sub>. Figure 7b presents the variation value of the refractive index, 2.32–2.00, as the temperature increased to 700 °C.

**Table 1.** The parameters obtained for WO<sub>3</sub> + 2% Fe layer samples grown at T = 600 °C and 4 h deposition time.

WO <sub>3</sub> + 2% Fe onto Sapphire Substrate, T = 600 °C, 4 h Deposition Time										
$\lambda$	$T_M$	$T_m$	$s$	$n_1$	$d_1$	$m_0$	$m$	$d_2$	$n_2$	$n_2$ Cauchy Dispersion
435	<u>0.782</u>	0.63	1.708	2.34		5.55	5	463.95	2.35	2.26
457	0.831	<u>0.73</u>	1.704	2.09	<del>820.76</del>	4.71	4.5	491.61	2.22	2.24
506	<u>0.968</u>	0.76	1.685	2.28	500.75	4.64	4	443.84	2.19	2.18
562	0.97	<u>0.803</u>	1.679	2.15	<del>699.78</del>	3.95	3.5	455.93	2.13	2.14
647	<u>0.98</u>	0.812	1.672	2.14	529.54	3.41	3	452.50	2.10	2.10
758	0.992	<u>0.824</u>	1.667	2.12	<del>642.9</del>	2.89	2.5	444.83	2.05	2.06
943	<u>0.993</u>	0.882	1.663	1.97		2.15	2	477.54	2.04	2.02
$d_1 = 515.15 \text{ nm} \pm 14.39 \text{ nm} \quad \delta = 2.8\%$										
$d_2 = 461.45 \text{ nm} \pm 6.67 \text{ nm} \quad \delta = 1.44\%$										
<b>SEM <math>d = 418.16 \text{ nm} \pm 17.28 \text{ nm} \quad \delta = 0.09\%</math>,</b>										
$n(\lambda) = 1.964 + \frac{0.5752 \cdot 10^5}{\lambda^2}$										

Note: The underlined values in the table are attached in this way to indicate that they are obtained from the transmission graph obtained by spectrophotometry. The other values are obtained from the envelope curves according to Swanepoel theory. The numbers in the table are cut to show that their values obtained from the experiment were not used in the calculation of the final value of  $n_2$  because they had very large deviations, well above the error limit.

**Table 2.** The parameters obtained for WO<sub>3</sub> + 2% Fe layer sample grown at T = 700 °C and 4 h deposition time.

WO <sub>3</sub> + 2% Fe onto Sapphire Substrate, T = 700 °C, 4 h Deposition Time										
$\lambda$	$T_M$	$T_m$	$s$	$n_1$	$d_1$	$m_0$	$m$	$d_2$	$n_2$	$n_2$ Cauchy Dispersion
454	<u>0.737</u>	0.589	1.7	2.38		5.50	5	475.33	2.32	2.22
473	0.807	<u>0.719</u>	1.69	2.04	414.4	4.53	4.5	519.2	2.18	2.19
529	<u>0.91</u>	0.766	1.68	2.14	637.27	4.24	4	493.47	2.17	2.14
585	0.941	<u>0.808</u>	1.67	2.07	548.88	3.71	3.5	493.1	2.10	2.11
675	<u>0.977</u>	0.818	1.67	2.12	531.17	3.29	3	477.41	2.07	2.07
792	0.977	<u>0.835</u>	1.66	2.06	486.16	2.73	2.5	479.35	2.03	2.03
981	<u>0.988</u>	0.84	1.66	2.07		2.21	2	473.15	2.01	2.00
$d_1 = 523.57 \text{ nm} \pm 6.36 \text{ nm} \quad \delta = 7.01\%$										
$d_2 = 487.28 \text{ nm} \pm 6.16 \text{ nm} \quad \delta = 1.26\%$										
<b>SEM <math>d = 456.95 \text{ nm} \pm 5.28 \text{ nm} \quad \delta = 1.15\%</math></b>										
$n(\lambda) = 1.947 + \frac{0.5636 \cdot 10^5}{\lambda^2}$										

Note: The underlined values are obtained from the transmission graph obtained by spectrophotometry; The other values are obtained from the envelope curves according to Swanepoel theory.

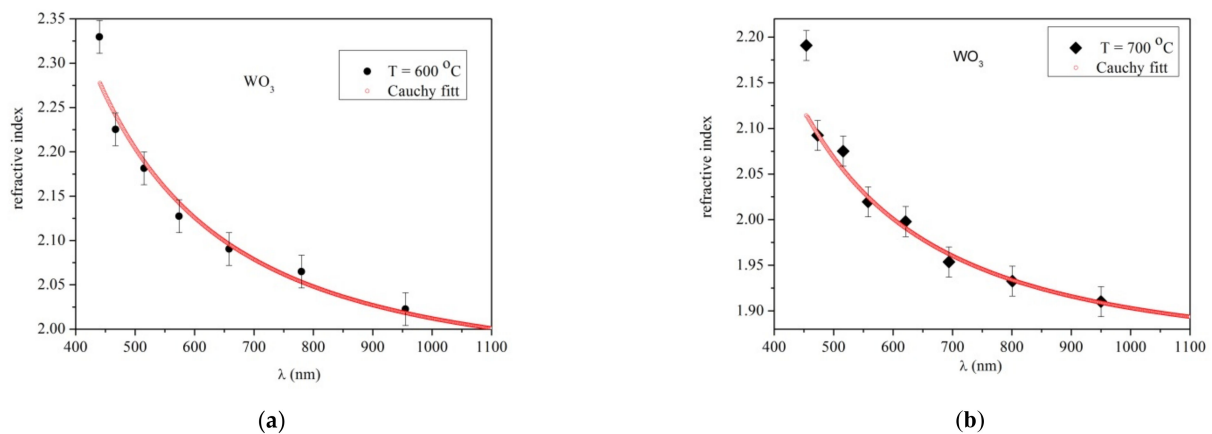


Figure 6. Refractive index plots of pure WO<sub>3</sub> layer grown at 4 h deposition time. (a) T = 600 °C; (b) T = 700 °C.

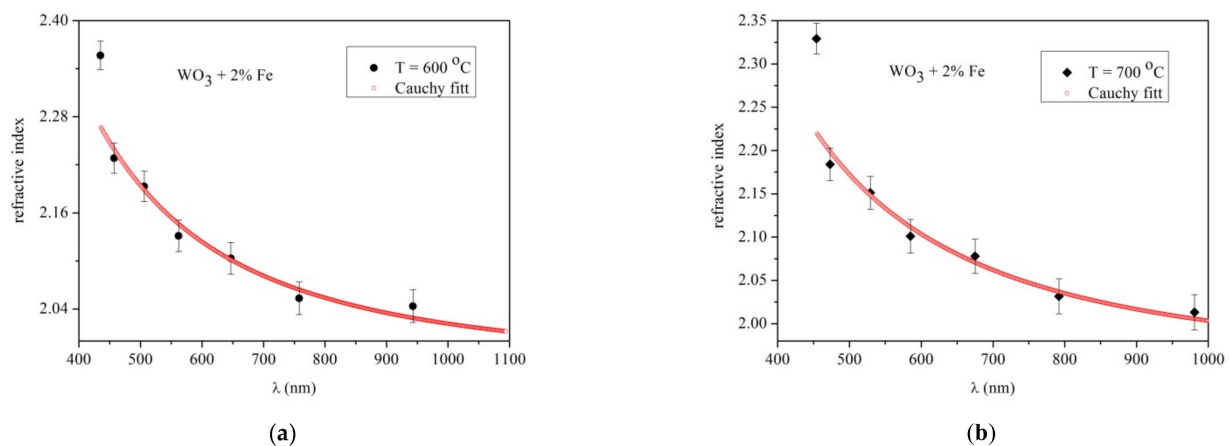
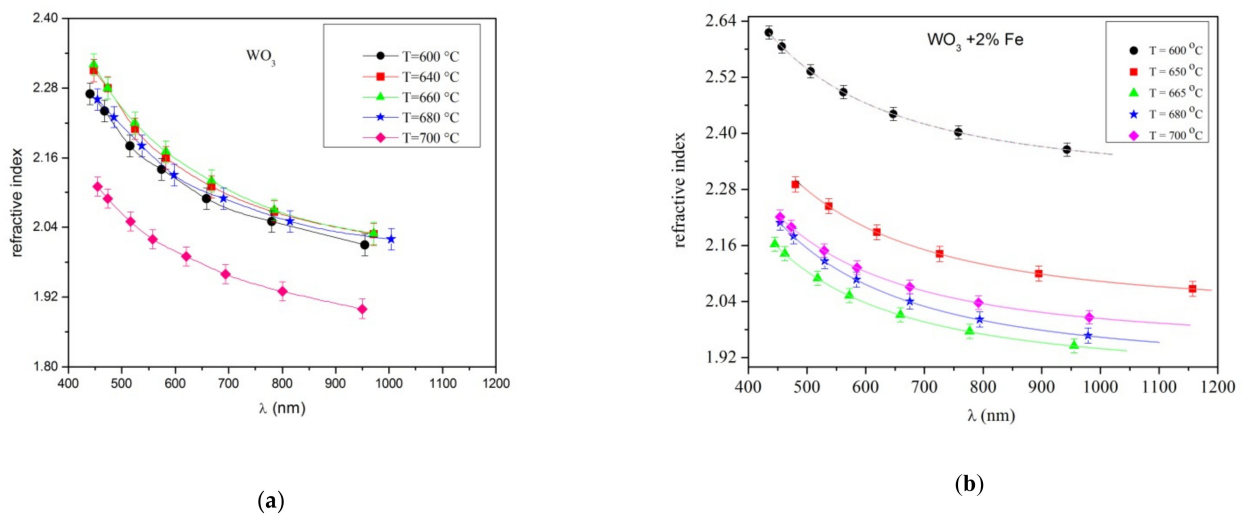


Figure 7. Refractive index plots for 2% Fe doped WO<sub>3</sub> layer grown at 4 h deposition time. (a) T = 600 °C; (b) T = 700 °C.

To understand the variation of the refractive index as the temperature increased, the plots of the refractive indexes are presented below, in Figure 8a,b. The refractive index presented in Figure 8a corresponds to a pure WO<sub>3</sub> layer, while that in Figure 8b corresponds to a 2% Fe-doped WO<sub>3</sub> layer, at temperatures in the 600–700 °C range.

In the Figure 8a the refractive index of pure WO<sub>3</sub> varied in the range of 2.40–2.14 for temperatures 600, 640, 660 and 680 °C, respectively. At a high temperature of 700 °C the refractive index has values from 2.16–1.92. A similar observation was found in [24–27]. This lower value of the refractive index could be explained by the self-annealing process that is activated at higher deposition time and substrate temperatures, the presence of the vacancies created in an atmosphere of oxygen during deposition. From Figure 8b, the variation of refractive index displayed values of 2.4–2.04 as the temperature increased. In the range of 600–700 °C, the refractive index values seems to have an approximately identical value within the error limits as the temperature increased. The refractive index of the layer grown at 640 °C has a high value, and it was supposed that around at 600–640 °C, at this critical temperature a change in the crystalline structure appeared. The X-ray measurements presented a random orientation of the monoclinic structure of the layer grown at 640 °C. In the hypothesized that since Fe has an atomic radius of 0.64 nm close to the size of W (0.62 nm), this can be introduced in a small quantities as a substitutional impurity in the WO<sub>3</sub> crystals causing a distortion of the crystal structure. Near to the oxygen vacancies considered in the WO<sub>3</sub> layer under high temperature, similar defects of the WO<sub>3</sub> lattice generated by Fe doping influenced the refractive index at 640 °C. Therefore, the presence of Fe in the host lattice of WO<sub>3</sub> could produce a mismatch of the lattice changing the properties of the film as well the type of strain during the growing process. It

is possible that at high temperature some formed Fe oxide bonds are broken since the layer surface is under the influence of the energetic species of the plasma.



**Figure 8.** The refractive index depending on the substrate temperatures. (a) pure WO<sub>3</sub> layer; (b) 2% Fe doped WO<sub>3</sub> layer.

To observe the effect of Fe-doped WO<sub>3</sub> on the refractive index, the measurements of 3% and 4% Fe-doped WO<sub>3</sub> were performed at 600 °C. Figure 9 show the refractive index of pure and Fe-doped WO<sub>3</sub>.

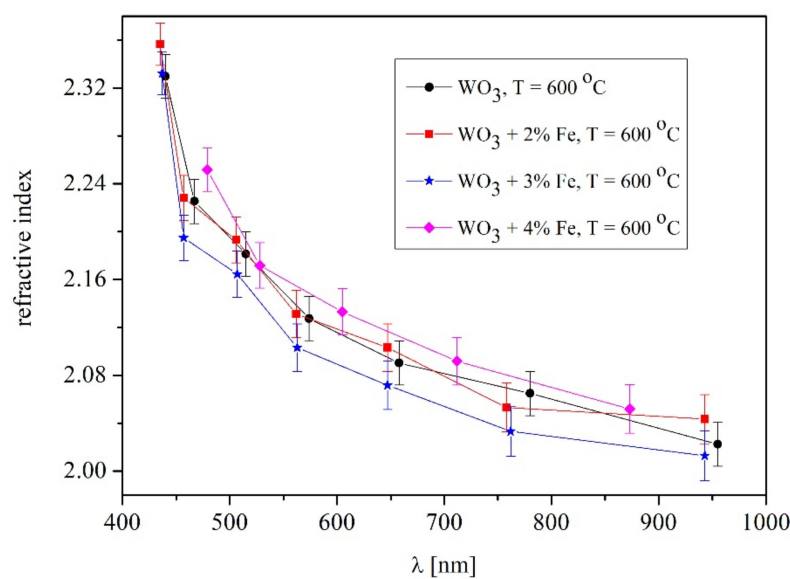


**Figure 9.** The refractive index of pure and Fe-doped WO<sub>3</sub> layers grown at 600 °C. The refractive index of pure WO<sub>3</sub> and 2, 3 and 4% Fe-doped WO<sub>3</sub> are compared.

From Figure 9, the refractive indexes for pure and 2% Fe-doped WO<sub>3</sub> seem to be nearly identical within the error limit, since these Fe percentages are considered smaller impurities in the WO<sub>3</sub> lattice. The refractive index of the 3% Fe-doped WO<sub>3</sub> is slightly smaller. It is worth mentioning that in case of the sapphire substrate, a few interference fringes exist in the transmittance spectra, thus the errors bars are high. Therefore, a decrease in the refractive index at 3% Fe in the host lattice of WO<sub>3</sub> is visible. The refractive index of 4% Fe-doped WO<sub>3</sub> is rising above the pure WO<sub>3</sub>. A first decrease in the refractive index and then an increase has been noticed for chalcogenide glasses with variation of Te content. As an explanation, such a variation of the refractive index was attributed to a large number

of defects, Te bindings in chalcogenide and the alteration of the valence band [27]. The changes in the refractive indexes of 3 and 4% Fe doped in  $\text{WO}_3$  are strongly related to the modification of crystalline structure observed in X-ray measurements (Figure 3a,b) and a few diffraction peaks vanished. Unlike 2% Fe doping, an increase in the content of Fe, defects, mismatches and distortions of the lattice became noticeable. Moreover, the defects of the  $\text{WO}_3$  lattice lead to a sub-stoichiometry and internal strain in the grown layer. The small amount of Fe changes the internal structure of the host lattice, leading to formation of a composition with a degree of disorder and higher localized state densities.

In Figure 10, the EDX measurements show the elemental species contained in the  $\text{WO}_3 + 2\%$  Fe layers at 600 °C and 680 °C, respectively. The temperature of 600 °C presents an amount of 0.23% Fe in the layer still smaller than it is in the target. The amount of Fe in the layer is shown in Table 3. It could be concluded that EDX measurements are not suitable for determination of the Fe content in these thin films.

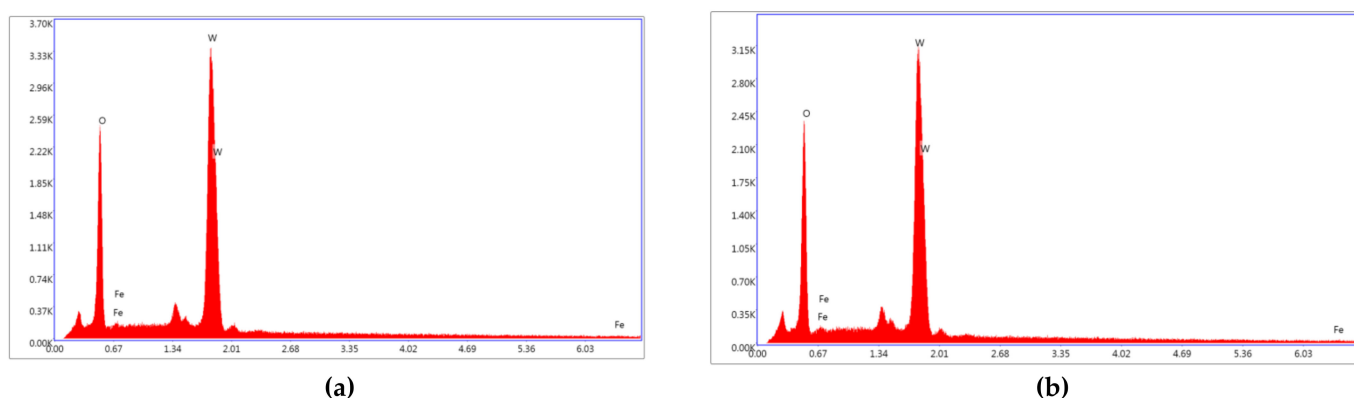


**Figure 10.** The EDX measurements for  $\text{WO}_3 + 2\%$  Fe grown at 4 h deposition time. (a)  $T = 600$  °C; (b)  $T = 680$  °C.

**Table 3.** The EDX species of the 2 %Fe doped  $\text{WO}_3$  and pure  $\text{WO}_3$  layers.

Temperatures (°C)	Layer	Element	Weight %	Atomic %	Intensity	Errors %
600 °C	$\text{WO}_3 + 2\%$ Fe	O (K)	16.86	69.86	143.59	6.14
		Fe (L)	0.19	0.23	0.62	66.09
		W (M)	82.95	29.91	266.03	3.34
680 °C	$\text{WO}_3 + 2\%$ Fe	O (K)	17.08	70.29	144.76	6.16
		Fe (L)	0.03	0.03	0.09	99.99
		W (M)	82.89	29.68	264.33	3.36
600 °C	$\text{WO}_3$	O (K)	17.36	70.70	77.31	6.94
		W(M)	82.64	29.30	138.36	4.09
660 °C	$\text{WO}_3$	O (K)	17.49	70.90	76.34	6.94
		W(M)	82.51	29.10	135.21	4.04

It is worth mentioning that in the case of a sapphire substrate it is possible that the little amount of the oxygen could be slightly higher since a part of it is coming from the substrate.

### 3.4. Optical Band Gap Measurements

The plots of  $(\alpha h\nu)^{1/2}$  versus  $h\nu$ , by Equation (4), for the  $\text{WO}_3$  samples grown at 4 h deposition time at two temperatures (600 and 700 °C, respectively) are presented in Figure 11a,b.

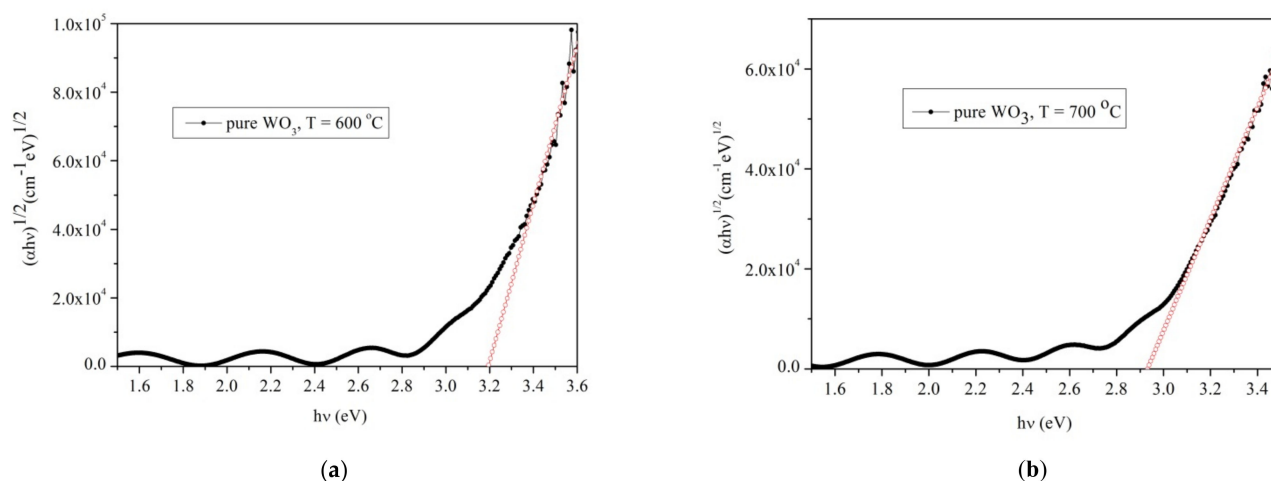
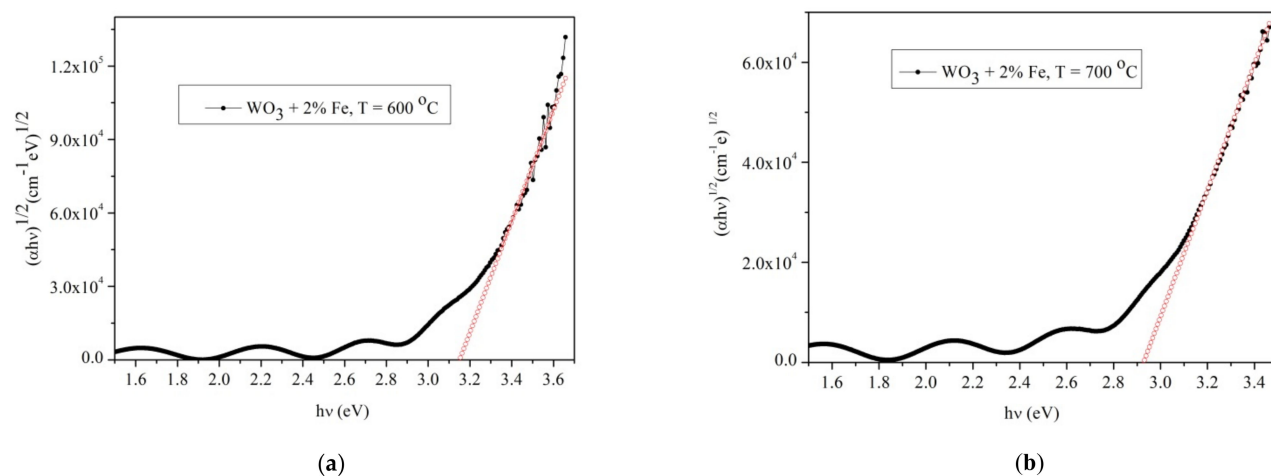


**Figure 11.** Optical band gap of pure  $\text{WO}_3$  layers grown on sapphire substrates: (a) sample at  $600\text{ }^\circ\text{C}$  (b) sample at  $700\text{ }^\circ\text{C}$ .

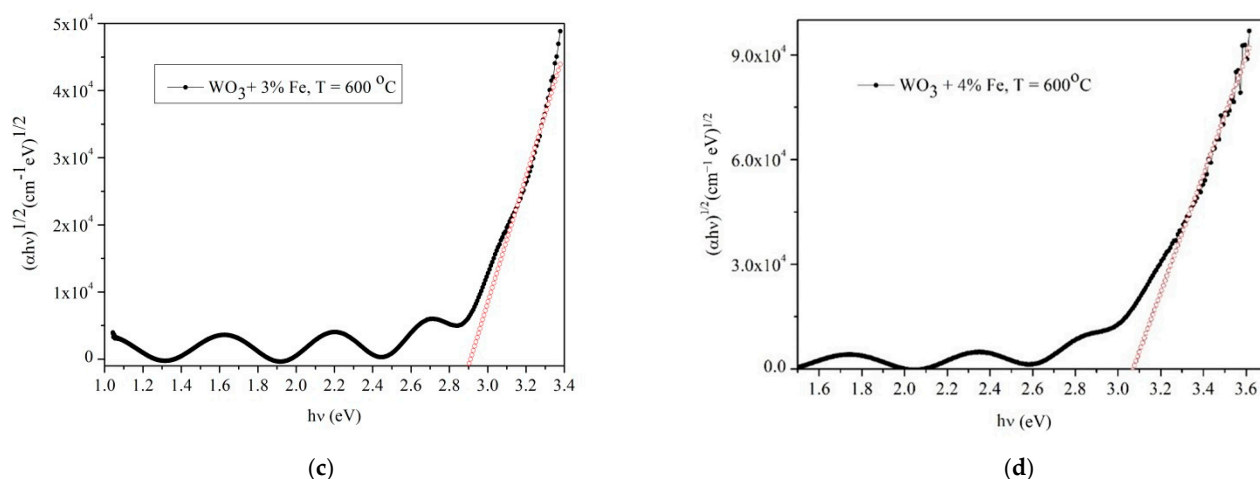
The energy band gap of  $\text{WO}_3$  layer is  $3.2\text{ eV}$  at  $600\text{ }^\circ\text{C}$ , while as the temperature increases to  $700\text{ }^\circ\text{C}$  the energy band gap becomes  $2.8\text{ eV}$ . This decrease in the energy is usual, since as the temperature increase the energy band gap became smaller.

Figure 12a–d show the energy band gap for Fe-doped  $\text{WO}_3$ . In Figure 12a,b, the energy band gap for 2% doped  $\text{WO}_3$  at  $600$  and  $700\text{ }^\circ\text{C}$  respectively, were presented. The energy band gap at  $600\text{ }^\circ\text{C}$  is  $3.18\text{ eV}$  while at  $700\text{ }^\circ\text{C}$  it is  $2.92\text{ eV}$ . Unlike pure  $\text{WO}_3$  the energy band gap of 2% Fe-doped  $\text{WO}_3$  has a small variation of approximately  $0.02\text{ eV}$  at  $600\text{ }^\circ\text{C}$  while at  $700\text{ }^\circ\text{C}$  it is nearly identical.

In Figure 12c,d the energy band gap of 3 and 4% Fe-doped  $\text{WO}_3$  at  $600\text{ }^\circ\text{C}$  is presented. The small change observed for pure and Fe-doped  $\text{WO}_3$  is mainly caused by the amount of Fe in the  $\text{WO}_3$  host lattice, leading to a small decrease in the value of the band gap. The optical band gap is strongly dependent on the amount of Fe atoms that have the tendency to enter in the lattice producing a physical disordering and creating localized states in the forbidden gap leading to a lower optical band gap. Therefore, a large number of charged defect states, induces structural changes in the host network, as it was observed in X-ray and SEM measurements and in the variation of the refractive index with temperature and amount of Fe. The increase of the Fe content leads to the formation of the composition and the densities of the localized states, so the small amount of Fe acts as an impurity center in the mobility gap. The distribution of the localized states is modified and new states are created in the mobility gap that change the optical band gap.



**Figure 12.** Cont.



**Figure 12.** Optical band gap of pure  $\text{WO}_3$  layers grown on sapphire substrates: (a) 2% Fe-doped  $\text{WO}_3$  at 600 °C; (b) 2% Fe-doped  $\text{WO}_3$  at 700 °C; (c) 3% Fe-doped  $\text{WO}_3$  at 600 °C; (d) 4% Fe-doped  $\text{WO}_3$  at 600 °C.

#### 4. Conclusions

The refractive index of pure and 2, 3 and 4% Fe-doped  $\text{WO}_3$  layers were calculated from the transmittance spectra by the Swanepoel method. The crystalline structure of 2, 3 and 4% Fe-doped  $\text{WO}_3$  showed a small shift compared with pure  $\text{WO}_3$ . The diffraction peaks at (022), (200), (040) and (400) vanished with the increase of Fe content in the  $\text{WO}_3$  host lattice at 600 °C. The nanocrystallite size measured from SEM images of the pure  $\text{WO}_3$  displayed a random variation with the increase of substrate temperature. Increasing the substrate temperature to 680 °C, the surface morphology of the grown films consists of pyramidal-shape grains, randomly oriented with respect to the substrate surface. A large amount of physical defects was observed, like micro-holes, visible around the grains as shown by SEM. Particularly at 700 °C, a surface morphology with rectangular-shaped grains was observed. The 2% Fe-doped  $\text{WO}_3$  presented an increase of the nanocrystallite size from 60 nm–197 nm as the substrate temperature increased between 600–700 °C. The morphology of the films has a “cobble” appearance, with well-defined grains at 600 °C. The films grown at temperatures of 650 °C and 680 °C had a rough surface morphology, composed of slightly larger pyramid-shaped crystallites and a large amount of physical defects like micro-porosity visible at the grain boundaries site. A 700 °C temperature leads to a compact surface morphology formed by large pyramidal-shaped grains and nano-porosity located on the grains’ surface.

The refractive index of pure  $\text{WO}_3$  at temperatures 600, 660, 660 and 680 °C, respectively had the identical values ranging from 2.4–2.04 while for 700 °C it decreases to 2.16–1.92 in the 400–1100 nm wavelength range. The value refractive index of 2% Fe-doped  $\text{WO}_3$  was 2.3–2.14 at 650 °C and slightly smaller (2.3–2.0) at 660, 680 and 700 °C, respectively. An increase to 3 and 4% Fe content in the  $\text{WO}_3$  lattice led to nearly identical values of the refractive index as pure and 2% Fe-doped  $\text{WO}_3$  at 600 °C. It was obvious that the 3% Fe content is slightly lower than 2% Fe-doped  $\text{WO}_3$  while at 4% Fe it is slightly higher than pure  $\text{WO}_3$ . Therefore, we presumed that the refractive index with Fe content variation could be considered nearly identical within the error limits at 600 °C. The modification of the refractive index with different Fe content in the  $\text{WO}_3$  lattice was in agreement with the changes in the crystalline structure observed by X-ray measurements.

The optical band gap varied with temperature for pure  $\text{WO}_3$  from 3.2 eV at 600 °C and 2.8 eV at 700 °C, respectively. The 2, 3 and 4% Fe-doped  $\text{WO}_3$  presented a small variation of optical band gap at 600 °C.

**Author Contributions:** Conceptualization, M.O., I.T. and I.B.; methodology, M.O.; software, M.-S.R. and M.J.; validation, M.O., I.B. and I.T.; formal analysis, M.-S.R.; investigation, M.O.; resources, M.J.;

data curation, M.O.; writing—original draft preparation, M.O.; writing—review and editing, I.B.; visualization, I.T.; supervision, M.O.; project administration, M.O.; funding acquisition, M.O. All authors have read and agreed to the published version of the manuscript.

**Funding:** This research was funded by Romanian National Authority for Scientific Research, UEFISCDI: project no. PCCDI 15; project name manufacture, Calibration and Testing of Advanced Integrated Sensor Systems for Societal Security.

**Institutional Review Board Statement:** Not applicable.

**Informed Consent Statement:** Not applicable.

**Data Availability Statement:** The data presented in this study are available on request from the corresponding author.

**Acknowledgments:** I.T., acknowledges support from the grant POCU/380/6/13/123990, financed by the European Social Fund within the Sectorial Operational Program Human Capital 2014–2020.

**Conflicts of Interest:** The authors declare no conflict of interest.

## References

1. Lethy, K.J.; Beena, D.; Kumar, R.V.; Pillai, V.M.; Ganesan, V.; Sathe, V. Structural, optical and morphological studies on laser ablated nanostructured WO<sub>3</sub> thin films. *Appl. Surf. Sci.* **2008**, *254*, 2369–2376. [[CrossRef](#)]
2. Datta, N.; Ramgir, N.; Kaur, M.; Roy, M.; Bhatt, R.; Kailasaganapathi, S.; Debnath, A.K.; Aswal, D.K.; Gupta, S.K. Vacuum deposited WO<sub>3</sub> thin films based sub-ppm H<sub>2</sub>S sensor. *Mater. Chem. Phys.* **2012**, *134*, 851–857. [[CrossRef](#)]
3. Shen, X.; Wang, G.; Wexler, D. Large-scale synthesis and gas sensing application of vertically aligned and double-sided tungsten oxide nanorod arrays. *Sens. Actuators B Chem.* **2009**, *143*, 325–332. [[CrossRef](#)]
4. Patel, K.J.; Panchal, C.J.; Kheraj, V.A.; Desai, M.S. Growth, structural, electrical and optical properties of the thermally evaporated tungsten trioxide (WO<sub>3</sub>) thin films. *Mater. Chem. Phys.* **2009**, *114*, 475–478. [[CrossRef](#)]
5. Qin, Y.; Hu, M.; Zhang, J. Microstructure characterization and NO<sub>2</sub>-sensing properties of tungsten oxide nanostructures. *Sens. Actuators B Chem.* **2010**, *150*, 339–345. [[CrossRef](#)]
6. Cho, M.-H.; Park, S.A.; Yang, K.-D.; Lyo, I.W.; Jeong, K.; Kang, S.K.; Ko, D.-H.; Kwon, K.W.; Ku, J.H.; Choi, S.Y.; et al. Evolution of tungsten-oxide whiskers synthesized by a rapid thermal-annealing treatment. *J. Vac. Sci. Technol. B* **2004**, *22*, 1084. [[CrossRef](#)]
7. Granqvist, C.G. Electrochromic tungsten oxide films: Review of progress 1993–1998. *Sol. Energy Mater. Sol. Cells* **2000**, *60*, 201–262. [[CrossRef](#)]
8. Niklasson, G.A.; Granqvist, C.G. Electrochromics for smart windows: Thin films of tungsten oxide and nickel oxide, and devices based on these. *J. Mater. Chem.* **2007**, *17*, 127–156. [[CrossRef](#)]
9. Brezesinski, T.; Rohlfling, D.F.; Sallard, S.; Antonietti, M.; Smarsly, B.M. Highly crystalline WO<sub>3</sub> thin films with ordered 3D mesoporosity and improved electrochromic performance. *Small* **2006**, *2*, 1203–1211. [[CrossRef](#)]
10. Bechinger, C.; Bullock, J.N.; Zhang, J.-G.; Tracy, C.E.; Benson, D.K.; Deb, S.K.; Branz, H.M. Low-voltage electrochromic device for photovoltaic-powered smart windows. *J. Appl. Phys.* **1996**, *80*, 1226–1232. [[CrossRef](#)]
11. Liu, K.; Foord, D.T.; Scipioni, L. Easy growth of undoped and doped tungsten oxide nanowires with high purity and orientation. *Nanotechnology* **2005**, *16*, 10–14. [[CrossRef](#)]
12. Yin, M.; Yu, L.; Liu, S. Synthesis of Ag quantum dots sensitized WO<sub>3</sub> nanosheets and their enhanced acetone sensing properties. *Mater. Lett.* **2017**, *186*, 66–69. [[CrossRef](#)]
13. Miu, D.; Birjega, R.; Viespe, C. Surface acoustic wave hydrogen sensors based on nanostructured Pd/WO<sub>3</sub> bilayers. *Sensors* **2018**, *18*, 3636. [[CrossRef](#)] [[PubMed](#)]
14. Palla-Papavlu, A.; Filipescu, M.; Schneider, C.W.; Antohe, S.; Ossi, P.M.; Radnóczy, G.; Dinescu, M.; Wokaun, A.; Lippert, T. Direct laser deposition of nanostructured tungsten oxide for sensing applications. *J. Phys. D Appl. Phys.* **2016**, *49*, 205101. [[CrossRef](#)]
15. Osiac, M.; Cioatera, N.; Jigau, M. Structural, Morphological and Optical Properties of Iron Doped WO<sub>3</sub> Thin Film Prepared by Pulsed Laser Deposition. *Coatings* **2020**, *10*, 412. [[CrossRef](#)]
16. Osiac, M.; Cioatera, N.; Udristiou, M.-T. The systemization of the tungsten oxide thin film used for gas sensor applications. In Proceedings of the AIP Conference Proceedings, Timisoara, Romania, 30 May 2019; Volume 2071, p. 040015.
17. Udristiou, M.-T.; Osiac, M. Au-incorporated in tungsten trioxide obtained by pulsed laser deposition. In Proceedings of the AIP Conference Proceedings, Timisoara, Romania, 20 May 2020; Volume 2218, p. 030012.
18. Swanepoel, R. Determination of the thickness and optical constants of amorphous silicon. *J. Phys. E Sci. Instrum.* **1983**, *16*, 1214–1222. [[CrossRef](#)]
19. Manifacier, J.C.; Gasiot, J.; Fillard, J.P. A simple method for the determination of the optical constants n, h and the thickness of a weakly absorbing thin film. *J. Phys. E Sci. Instrum.* **1976**, *9*, 1002–1004. [[CrossRef](#)]
20. Poelman, D.; Smet, P.F. Methods for the determination of the optical constants of thin films from single transmission measurements: A critical review. *J. Phys. D Appl. Phys.* **2003**, *36*, 1850–1857. [[CrossRef](#)]

21. Gonzalez-Leal, J.-M.; Prieto-Alcon, R.; Angel, J.-A.; Minkov, D.A.; Marquez, E. Influence of substrate absorption on the optical and geometrical characterization of thin dielectric films. *Appl. Optics* **2002**, *41*, 7300–7308. [[CrossRef](#)]
22. Shannon, R.D. Revised effective ionic radii and systematic studies of interatomic distances in halides and chalcogenides. *Acta Cryst.* **1976**, *32*, 751–767. [[CrossRef](#)]
23. Cornell, R.M.; Schwertmann, U. *The Iron Oxides: Structures, Properties, Reactions, Occurrences and Uses*, 2nd ed.; WILEY-VCH: Weinheim, Germany, 2003; pp. 253–296.
24. Tirca, I.; Boerasu, I.; Radu, M.-S.; Osiac, M. Refractive index of WO<sub>3</sub> thin films grown under various temperatures determined by the Swanepoel method. *Phys. B* **2021**, accepted.
25. Lethy, K.J.; Beena, D.; Kumar, R.V.; Pillai, V.P.M.; Ganesan, V.; Sathe, V.; Phase, D.M. Nanostructured tungsten oxide thin films by the reactive pulsed laser deposition technique. *Appl. Phys. A* **2008**, *91*, 637–649. [[CrossRef](#)]
26. Ouni, B.; Boukhachem, A.; Dabbous, S.; Amlouk, A.; Boubaker, K.; Amlouk, M. Some transparent semi-conductor metal oxides: Comparative investigations in terms of Wemple–DiDomenico parameters, mechanical performance and Amlouk–Boubaker opto-thermal expansivity. *Mater. Sci. Semicond. Process.* **2010**, *13*, 281–287. [[CrossRef](#)]
27. Sharma, P.; Katyal, S.C. Optical study of Ge<sub>10</sub>Se<sub>90–x</sub>Te<sub>x</sub> glassy semiconductors. *Thin Solid Film.* **2007**, *515*, 7966–7970. [[CrossRef](#)]